Mitochondria-driven assembly of a cortical anchor for mitochondria and dynein

Lauren M. Kraft and Laura L. Lackner

Department of Molecular Biosciences, Northwestern University, Evanston, IL

Interorganelle contacts facilitate communication between organelles and impact fundamental cellular functions. In this study, we examine the assembly of the MECA (mitochondria–endoplasmic reticulum [ER]–cortex anchor), which tethers mitochondria to the ER and plasma membrane. We find that the assembly of Num1, the core component of MECA, requires mitochondria. Once assembled, Num1 clusters persistently anchor mitochondria to the cell cortex. Num1 clusters also function to anchor dynein to the plasma membrane, where dynein captures and walks along astral microtubules to help orient the mitotic spindle. We find that dynein is anchored by Num1 clusters that have been assembled by mitochondria. When mitochondrial inheritance is inhibited, Num1 clusters are not assembled in the bud, and defects in dynein-mediated spindle positioning are observed. The mitochondria-dependent assembly of a dual-function cortical anchor provides a mechanism to integrate the positioning and inheritance of the two essential organelles and expands the function of organelle contact sites.

Introduction

As the number and diversity of newly discovered interorganelle contacts increase, it is clear that these contacts impact many aspects of cell biology (Helle et al., 2013; Prinz, 2014; Eisenberg-Bord et al., 2016; Gatta and Levine, 2017; Kraft and Lackner, 2017). Many proteins and protein complexes that function to directly tether organelles have been identified (Prinz, 2014; Eisenberg-Bord et al., 2016; Gatta and Levine, 2017). Some serve solely to physically bridge organelles, whereas others actively participate in interorganelle communication and function. Importantly, these proteins establish, maintain, and alter contacts in response to different physiological contexts. Thus, gaining an understanding of the tethering mechanism, activity, and regulation of these proteins provides insight into how interorganelle contacts and their critical functions are regulated.

In budding yeast, the mitochondria–ER–cortex anchor (MECA) functions to tether mitochondria to the cortical ER and plasma membrane, bringing the three cellular membranes in close proximity (Cerveny et al., 2007; Hammermeister et al., 2010; Klecker et al., 2013; Lackner et al., 2013; Ping et al., 2016). MECA interacts directly with mitochondria and the plasma membrane via two distinct lipid-binding domains within its core protein component, Num1. A membrane-binding region within the N-terminal coiled-coil (CC) region of Num1 interacts directly with the mitochondrial outer membrane (MOM; Tang et al., 2012; Lackner et al., 2013; Ping et al., 2016), and a C-terminal pleckstrin homology domain interacts with $PI_{4,5}P_2$ in the plasma membrane (Yu et al., 2004; Tang et al., 2009). Num1CC also mediates Num1 self-interactions and is required for Num1 to assemble into clusters at the cell cortex (Tang et al., 2012; Lackner et al., 2013). Mutations that interfere with the ability of Num1 to assemble into clusters decrease the tethering capacity of MECA, suggesting that assembly of Num1 increases the avidity of Num1 for its target membranes (Lackner et al., 2013; Ping et al., 2016). Therefore, the regulation of Num1 assembly likely serves as a mechanism to regulate the tethering function of MECA.

In addition to functioning as a cortical anchor for mitochondria, Num1 plays a well-characterized role as a cortical anchor for dynein (Heil-Chapdelaine et al., 2000; Farkasovsky and Küntzel, 2001; Markus and Lee, 2011). At the cell cortex, dynein captures and walks along astral microtubules, generating a pulling force to position the mitotic spindle across the mother–bud neck during mitosis (Eshel et al., 1993; Li et al., 1993; Adames and Cooper, 2000). Mutants that interfere with Num1 assembly exhibit compromised dynein activity (Tang et al., 2012). Together, these observations suggest that Num1 assembly strengthens its interaction with all binding partners, including dynein and phospholipid membranes. Whereas Num1 assembly facilitates its function as an anchor for mitochondria and dynein, factors influencing Num1 assembly are poorly understood. Here, we report that the assembly of Num1 requires an interaction with mitochondria. Additionally, we find that mitochondria-assembled Num1 clusters function as cortical attachment sites for dynein and that disrupting

Correspondence to Laura L. Lackner: Laura.Lackner@northwestern.edu

Abbreviations used: AID, auxin-inducible degron; CC, coiled-coil; MECA, mitochondria–ER–cortex anchor; MOM, mitochondrial outer membrane; ROI, region of interest; SC, synthetic complete; YP, yeast extract/peptone.

The Rockefeller University Press
J. Cell Biol. Vol. 216 No. 10 3061–3071
https://doi.org/10.1083/jcb.201702022

mitochondria-driven assembly of Num1 leads to defects in dynein-mediated spindle positioning.

Results and discussion

Num1 clusters are stable and persistently associated with mitochondria

Num1 exists in clusters at the cell cortex as well as in a pool that is diffusely localized along the plasma membrane and with cortical ER (Farkasovsky and Küntzel, 1995; Heil-Chapdelaine et al., 2000; Lackner et al., 2013; Chao et al., 2014). To examine the relationship between Num1 clusters and mitochondria, we imaged live cells expressing Num1-yEGFP and mitochondrial matrix–targeted dsRED (mitoRED). Quantification of Num1 clusters and their mitochondrial association revealed that ∼98% of Num1 clusters are mitochondrially associated over time (Fig. 1, A and B). In addition, mitochondria-associated clusters were stationary, exhibiting limited movement along the cell cortex for the duration of imaging (Fig. 1, C and E; Heil-Chapdelaine et al., 2000). To examine the dynamics of protein exchange within a Num1 cluster, we used FRAP. After the photobleaching of a mitochondria-associated Num1 cluster, minimal recovery of the Num1-yEGFP signal was observed 21 min after photobleaching (Fig. 1, C and D). Thus, Num1 clusters are persistent, stationary, and display limited exchange with the nonassembled pool of Num1.

Num1 cluster formation requires mitochondria

As shown above, nonmitochondrial Num1 clusters are rarely observed (Fig. 1, A and B). The region of Num1 that is required for cluster formation, Num1CC, interacts with itself and directly with mitochondria (Tang et al., 2012; Lackner et al., 2013; Ping et al., 2016), suggesting these activities may be interdependent. To test this idea, we visualized Num1 cluster formation in live cells. Early in the cell cycle, mitochondria are inherited (Simon et al., 1997), but buds are devoid of Num1 clusters. As the cell cycle progresses and buds increase in size, Num1 clusters are readily observed (Farkasovsky and Küntzel, 1995; Heil-Chapdelaine et al., 2000). Using long-term imaging of asynchronous cell populations, we captured the formation of Num1 clusters in the growing bud and observed that clusters form on areas of the cell cortex that are in close proximity to mitochondria (Fig. 1 E). These results suggest that the formation of Num1 clusters is dependent on an interaction with mitochondria.

If mitochondria are indeed required for Num1 cluster formation, cells devoid of mitochondria should lack Num1 clusters. To test this, we used a well-characterized temperature-sensitive mitochondrial inheritance mutant, *mmr1-5* Δ*ypt11*, which will be referred to as *mito*^{ts} (Chernyakov et al., 2013). Mmr1 and Ypt11 function as adapters that link mitochondria to Myo2, a type V myosin that drives actin-based transport of mitochondria to the bud (Itoh et al., 2002, 2004; Boldogh et al., 2004; Altmann et al., 2008; Frederick et al., 2008; Förtsch et al., 2011; Eves et al., 2012; Chernyakov et al., 2013). Active mitochondrial inheritance requires Myo2 and either Mmr1 or Ypt11. Thus, when *mito*^{ts} cells are grown at the nonpermissive temperature, the vast majority of buds are devoid of mitochondria, and, consequently, the cells exhibit a severe defect in growth (Chernyakov et al., 2013). The inheritance defect in *mito*^{ts} cells is specific to mitochondria; defects in the polarization of secretory vesicles, an essential function of Myo2 (Schott et al., 1999), and the inheritance of ER, a Myo4-dependent process, are not observed (Chernyakov et al., 2013).

We examined mitochondrial inheritance and Num1 cluster formation in WT and *mito*^{ts} cells expressing Num1-yEGFP and mitoRED at permissive (24°C) and nonpermissive (37°C) temperatures. In WT cells grown at 24°C and 37°C and *mito*^{ts} cells grown at 24°C, mitochondria were observed in both small and large buds, whereas Num1 clusters were predominantly absent in small buds and detected in large buds (Fig. 2, A–C), consistent with previous studies (Farkasovsky and Küntzel, 1995; Heil-Chapdelaine et al., 2000). In contrast, both mitochondria and Num1 clusters were absent in the majority of large buds of *mito*^{ts} cells grown at 37°C (Fig. 2 D). Importantly, the small percentage of Num1 clusters observed in large buds of *mito*^{ts} cells grown at 37°C was associated with mitochondria. The percentage of Num1 clusters associated with mitochondria and the number of Num1 clusters per mother cell were similar between WT and *mito*^{ts} cells at permissive and nonpermissive temperatures (Fig. 2, E and F), indicating that the *mito*^{ts} strain does not have a general defect in Num1 cluster assembly. Results similar to those obtained for the *mito*^{ts} mutant were obtained using *myo2-14*, a different temperature-sensitive mitochondrial inheritance mutant (Fig. S1; Schott et al., 1999; Santiago-Tirado et al., 2011; Chernyakov et al., 2013). Together, these data indicate that Num1 cluster formation is dependent on mitochondria.

Dynein is anchored to the cell cortex by mitochondria-assembled Num1 clusters

In addition to functioning as a cortical anchor for mitochondria, Num1 plays a well-characterized role as a cortical anchor for dynein. The CC region of Num1 is required for both the Num1–mitochondria and Num1–dynein interactions (Tang et al., 2012; Lackner et al., 2013). Whereas our data indicate that mitochondria are required for Num1 cluster formation, evidence indicates that Num1 cluster formation and maintenance do not require dynein. Specifically, Num1 clusters are observed to tether mitochondria in cells that lack dynein (Tang et al., 2012; Lackner et al., 2013), and a mutation in Num1 that abolishes the Num1–dynein interaction, Num1$^{L167E+L170E}$, does not interfere with Num1 cluster formation or mitochondrial tethering (Tang et al., 2012).

Our results, in combination with those of others described above, suggest a model in which dynein is anchored to the cell cortex by mitochondria-assembled Num1 clusters. To test this, we first examined whether Num1 clusters are able to simultaneously anchor mitochondria and dynein to the cell cortex. To facilitate long-term imaging of dynein, we fused mKate to the C terminus of Dyn1, the dynein heavy chain, and expressed the fusion protein from its endogenous locus. Cells expressing Dyn1-mKate exhibited no defects in spindle positioning and no growth defects in the absence of Kar9, a protein required for cell viability in the absence of dynein function, indicating Dyn1-mKate is functional (Fig. S2; Eshel et al., 1993; Li et al., 1993; Miller and Rose, 1998; Yin et al., 2000). In cells expressing Dyn1-mKate along with Num1-yEGFP and mitochondrial matrix–targeted TagBFP (mitoBFP), we observed mitochondria present at sites of Num1-Dyn1 colocalization (Fig. 3 A). Specifically, we found that the vast majority of cortical dynein foci (100 out of 112 cortical dynein foci; 89.3%) colocalize with both mitochondria and Num1, indicating that a Num1 cluster can simultaneously anchor mitochondria and dynein. In further

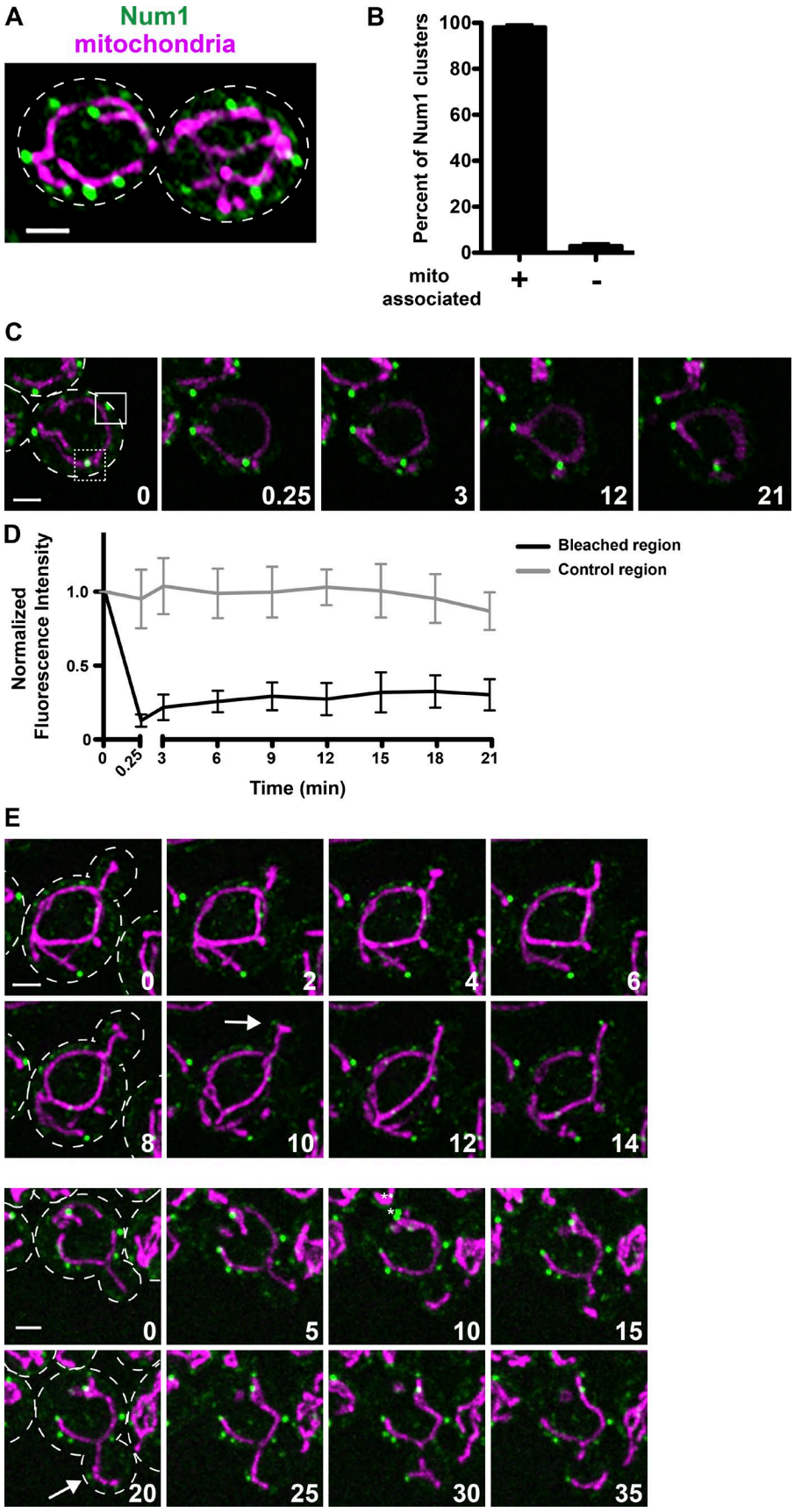

Figure 1. **Num1 clusters are stable and persistently associated with mitochondria.** (A) Cells expressing Num1-yEGFP and mitoRED were visualized by fluorescence microscopy. A whole-cell projection is shown. The cell cortex is outlined with a dashed line. (B) Quantification of mitochondria-associated Num1 clusters as shown in A. To be considered a mitochondria-associated cluster, mitochondria had to remain associated with a Num1 cluster for ≥1.5 min. $n = 5$ independent time-lapse series; $n \geq 69$ clusters per time-lapse series. The mean ± SD is shown. (C) Cells expressing Num1-yEGFP and mitoRED were photobleached, and the fluorescence recovery was visualized by fluorescence microscopy over time. Whole-cell projections are shown. Time is in minutes. Time 0 = prebleach. The quantified photobleached region is outlined with a solid line. The quantified control region is outlined with a dotted line. The cell cortex is outlined with a dashed line. (D) Quantification of fluorescence intensity over time for 10 photobleached and control regions as shown in C. Fluorescence intensities were normalized to the prebleach value. The mean ± SD is shown. For all recovery time points (time = ≥0.25 min), the difference between the control and bleached samples is statistically significant with p-values <0.0001. (E) Cells expressing Num1-yEGFP and mitoRED were visualized by fluorescence microscopy over time. Whole-cell projections are shown. Arrows indicate a forming tether point. Time is in minutes. The cell cortex is outlined with a dashed line in both rows for clarity. Asterisks in time = 10 min of the bottom time course denote hot pixels. Bars, 2 µm.

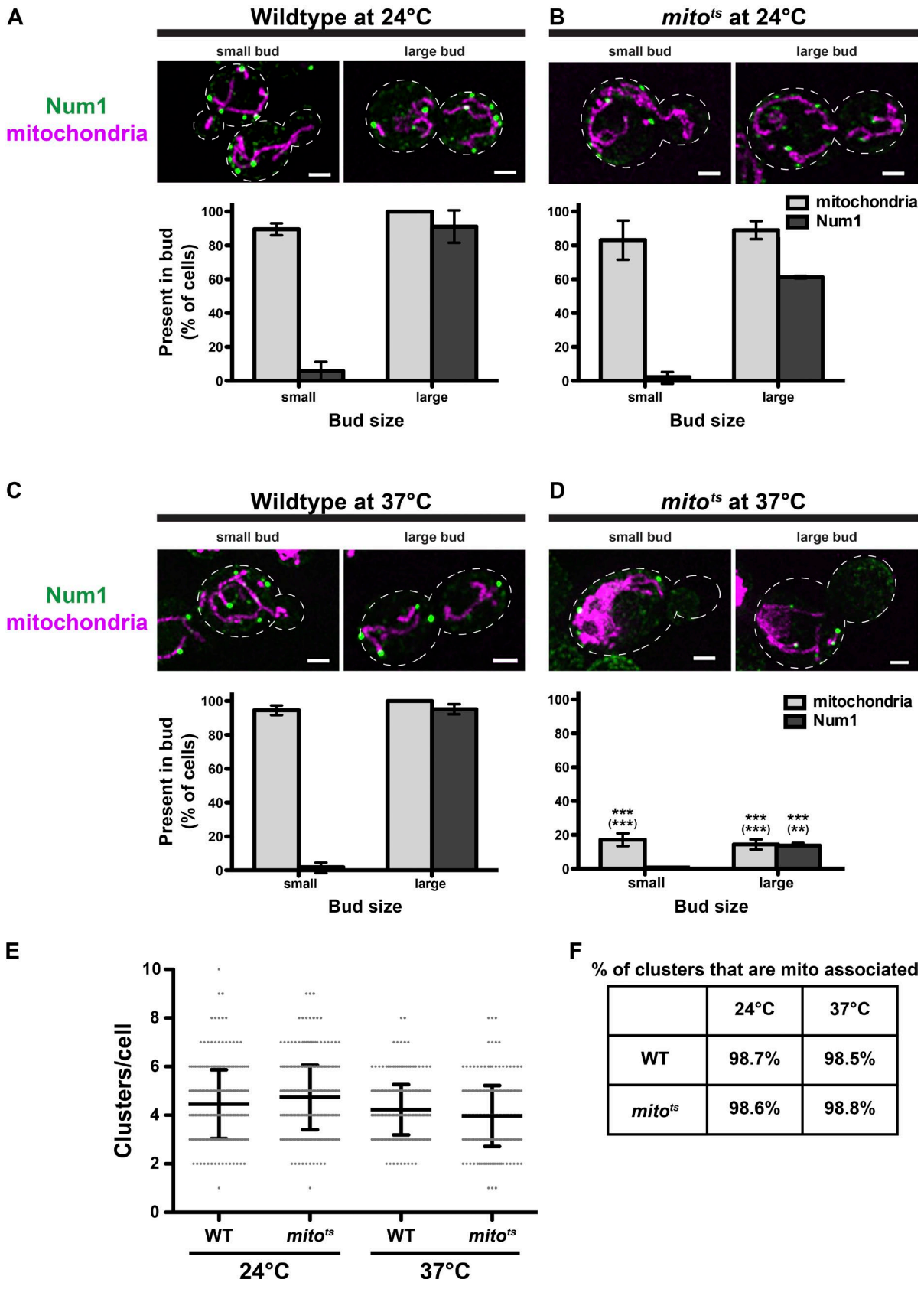

Figure 2. **Num1 cluster formation requires mitochondria.** (A–D) WT (A and C) and *mito*^{ts} (B and D) cells expressing Num1-yEGFP and mitoRED were grown at 24°C (A and B) and 37°C (C and D) and visualized by fluorescence microscopy. Representative whole-cell projections are shown. The cell cortex is outlined with a dashed line. Bars, 2 µm. The presence of mitochondria and assembled Num1 in buds was quantified for small and large buds. Buds were classified as follows: small buds have a bud/mother diameter ratio of <1:3, and large buds have a bud/mother diameter ratio of ≥1:3. *n* = 3 independent

support of the idea that dynein is anchored to the cell cortex by mitochondria-assembled Num1 clusters, we observed dynein colocalizing with existing Num1 clusters over time (Fig. 3 B), which our data indicate are assembled by mitochondria. In all 10 of the events in which we captured dynein becoming anchored at the cell cortex, dynein was found to colocalize with an existing Num1 cluster. These data indicate that a single mitochondria-assembled Num1 cluster can simultaneously anchor mitochondria and dynein, indicating that dynein-specific Num1 clusters are not required.

Defects in mitochondrial inheritance impair dynein-dependent spindle positioning

Cells expressing a Num1 mutant defective in cluster formation exhibit defects in dynein-mediated spindle positioning (Tang et al., 2012), indicating that Num1 cluster formation enhances cortical dynein function. Our data indicate that Num1 cluster formation requires mitochondria. Therefore, dynein function should be disrupted in cells that lack mitochondria. To test this, we examined how defects in mitochondrial inheritance affect the function of dynein in spindle positioning. We expressed Ruby-Tub1 and mitoBFP to visualize mitotic spindles and mitochondria in WT and *mito^{ts}* cells grown at the permissive and nonpermissive temperatures. In large budded cells, spindles >1.25 µm were scored as correctly oriented or misoriented (Moore et al., 2008). Examples of each are shown in Fig. 4 A. In comparison with WT cells grown at 24°C and 37°C and *mito^{ts}* cells grown at 24°C, *mito^{ts}* cells grown at 37°C exhibited a significant increase in the percentage of cells with misoriented spindles (Fig. 4 B). In fact, the percentage of cells with misoriented spindles in *mito^{ts}* cells grown at 37°C was comparable with that observed in Δ*num1* and Δ*dyn1* cells, supporting the idea that Num1 cluster formation and dynein function are disrupted. We also observed a slight but significant increase in spindle misorientation in Δ*mmr1* cells, which is likely a consequence of delayed mitochondrial inheritance in this strain (Itoh et al., 2004). In the absence of Kar9, a protein that functions in a partially redundant spindle positioning pathway, the percentage of *mito^{ts}* cells with misoriented spindles at 37°C was significantly increased compared to those with Kar9 (Fig. 4, B and C). These results suggest that defects in mitochondrial inheritance primarily affect dynein-mediated spindle positioning and not Kar9-mediated spindle positioning.

We also observed an increase in the percentage of cells with misoriented spindles in cells lacking Mdm36, the other known protein component of MECA (Fig. 4 B). Mdm36 is proposed to directly bridge interactions between Num1 dimers to facilitate Num1 cluster formation (Lackner et al., 2013). In the absence of Mdm36, Num1 is localized in smaller/less intense clusters, and the number of Num1-mediated mitochondrial tether points is reduced (Hammermeister et al., 2010; Lackner et al., 2013; Ping et al., 2016). Therefore, the spindle positioning defect observed in the absence of Mdm36 is consistent with the idea that Num1 cluster formation enhances cortical dynein function.

In addition to using a temperature-sensitive mitochondrial inheritance mutant in the BY4741 background, we constructed a mitochondrial inheritance mutant using the auxin-inducible degron (AID) system in the W303 background (Nishimura et al., 2009; Morawska and Ulrich, 2013). We noted that, in comparison with WT BY4741, the population of WT W303 cells contained a higher percentage of cells with misoriented spindles, as quantified by our spindle orientation scoring method (Fig. 4, B and E). The reason for the differences in spindle misorientation between the two WT genetic backgrounds is at this point unclear. In the W303 background, we tagged *MMR1* with the AID tag at its endogenous locus in Δ*ypt11* cells expressing Tir1, a plant-specific F-box protein. This strain is referred to as *mito^{AID}*. Tir1 binds the yeast SCF (Skp1, Cullen, F-box) complex and, in the presence of auxin, recruits the SCF complex to AID-tagged proteins, which are subsequently ubiquitinated and targeted for proteasomal degradation (Nishimura et al., 2009). When grown in the presence of auxin, the steady-state level of Mmr1 in *mito^{AID}* cells was dramatically reduced (Fig. S3 A). In addition, the cells exhibited severe defects in mitochondrial inheritance and growth consistent with the loss of both Myo2 mitochondrial adapters (Fig. S3, B and C; Frederick et al., 2008; Chernyakov et al., 2013). We also analyzed Num1 clusters in *mito^{AID}* cells 30 min after auxin treatment ($n \geq 102$ cells). In both auxin-treated and untreated samples, we found a mean of 4.5 Num1 clusters per mother cell and that the number of mitochondria-associated Num1 clusters were similar to WT cells (Fig. 1 B and Fig. S3, D and E). These results indicate that the rapid depletion of Mmr1 and consequent disruption of Mmr1 activity do not affect already formed Num1 clusters.

We analyzed spindle orientation in *mito^{AID}* cells expressing Ruby-Tub1 and mitochondrial matrix–targeted GFP (mitoGFP) in the absence or presence of auxin (Fig. 4 D). In comparison with WT cells and *mito^{AID}* cells grown in the absence of auxin, *mito^{AID}* cells grown in the presence of auxin exhibited a significant increase in the number of cells with misoriented spindles (Fig. 4 E). The number of misoriented spindles was similar to that observed in cells lacking dynein (Fig. 4 E) and was further increased in the absence of Kar9 (Fig. 4 F). Thus, in both the *mito^{ts}* and *mito^{AID}* cells, defects in mitochondrial inheritance correlated with defects in dynein-mediated spindle positioning. To test whether mitochondrial function is required for dynein's function in spindle positioning, we analyzed spindle orientation in rho^0 cells, which lack mitochondrial DNA. In rho^0 cells, the percentage of Num1 clusters associated with mitochondria (97.5%; $n = 439$ clusters) and the number of misoriented spindles were similar to WT (Fig. 4 E). These results indicate that Num1-mediated anchoring of mitochondria and dynein's function in spindle positioning do not require mitochondrial function.

We also assessed how defects in mitochondrial inheritance affect dynein function using a spindle oscillation assay, which is a more sensitive assay of dynein function. In the assay, dynein-mediated spindle movement is examined in hydroxyurea-arrested cells and, consequently, in the absence of spindle elongation (Moore et al., 2009; Tang et al., 2012). We analyzed spindle oscillations in hydroxyurea-arrested WT, Δ*dyn1*, and *mito^{ts}* cells at the permissive and nonpermissive temperature (Fig. 4 G). As expected, the percentage of spindles that crossed the mother–bud neck was decreased in Δ*dyn1* cells in comparison with WT cells. We also observed a decrease in spindle oscil-

experiments of >30 cells for each bud size. For A–D, the p-values are in comparison with WT cells at 37°C (no parentheses) or *mito^{ts}* cells at 24°C (parentheses); **, P < 0.01; ***, P < 0.001. (E and F) Quantification of the number of Num1 clusters per mother cell (E) and mitochondria-associated Num1 clusters (F) in WT and *mito^{ts}* cells at the indicated temperature. $n \geq 254$ cells. Each dot represents a cell. The mean ± SD is shown.

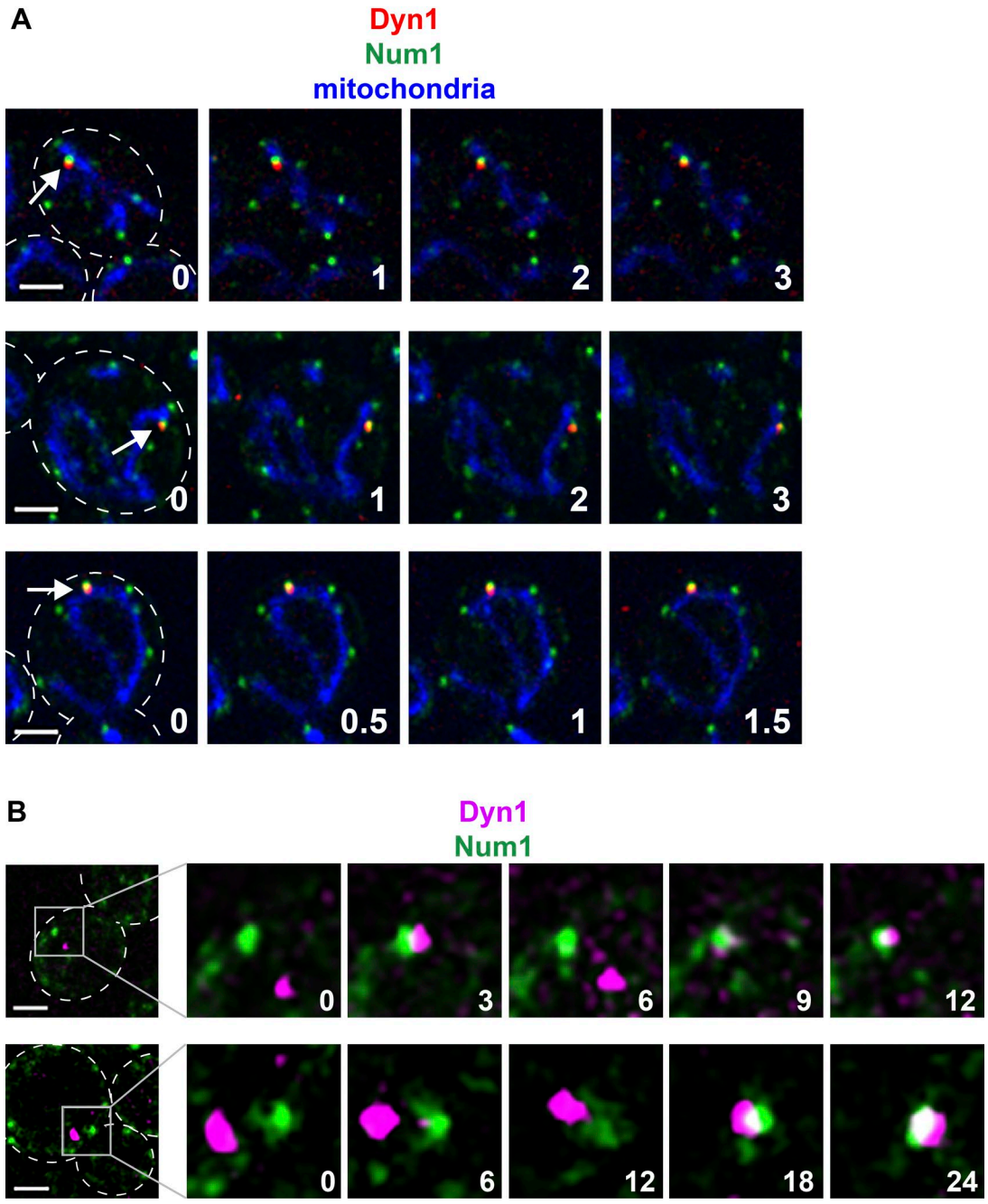

Figure 3. **Dynein associates with mitochondria-assembled Num1 clusters.** (A) WT cells expressing Num1-yEGFP, Dyn1-mKate, and mitoBFP were visualized by fluorescence microscopy over time. Representative whole-cell projections are shown. Arrows indicate a colocalization event. The cell cortex is outlined with a dashed line. (B) Cells expressing Num1-yEGFP and Dyn1-mKate were visualized by fluorescence microscopy over time. Representative partial-cell projections are shown. The cell cortex is outlined with a dashed line. The boxed area is magnified 3.3-fold. For the images shown, all Num1 clusters are cortical. Note that although some Num1 clusters may not appear to be cortical, this is a consequence of displaying the images as maximum intensity projections. Time is in minutes. Bars, 2 µm.

lation in *mito*^{ts} cells at the nonpermissive temperature. Due to the fact that 14% of buds in the hydroxyurea-arrested *mito*^{ts} cells inherit mitochondria at 37°C, the percentage of spindles observed to cross the mother–bud neck was even further decreased when only considering the population of *mito*^{ts} cells that lack mitochondria in the bud (Fig. 4 G). These results indicate that dynein function is compromised when buds do not inherit mitochondria and are consistent with the model in which dynein is anchored to the cell cortex by mitochondria-assembled Num1 clusters.

Here, we provide evidence demonstrating that mitochondria drive the assembly of Num1 clusters, which in turn serve to stably anchor the organelle itself as well as dynein to the plasma membrane (Fig. 5). Assembly of Num1 likely enhances interactions with its membrane and protein-binding partners and, consequently, the ability of Num1 to robustly tether mitochondria and dynein to the cell cortex. Thus, regulated assembly provides a mechanism to spatially and temporally control tether function. This fundamental mechanism of regulation likely extends be-

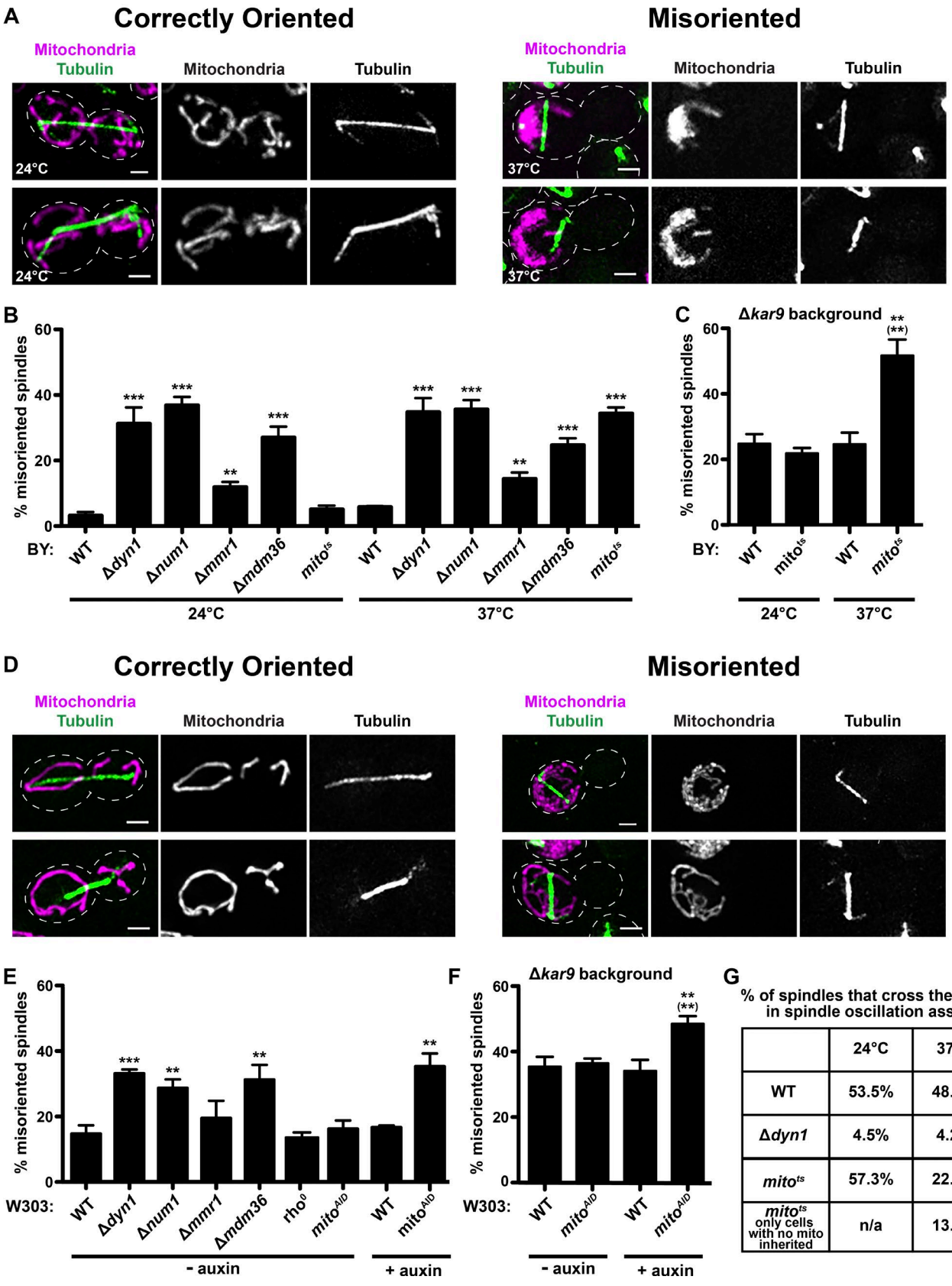

	24°C	37°C
WT	53.5%	48.3%
Δdyn1	4.5%	4.2%
mitots	57.3%	22.9%
mitots only cells with no mito inherited	n/a	13.9%

Figure 4. **Mitochondrial inheritance mutants exhibit defects in dynein-mediated spindle positioning.** (A–C) WT BY4741, Δ*dyn1*, Δ*num1*, Δ*mmr1*, Δ*mdm36*, Δ*kar9*, *mito*^{ts}, and *mito*^{ts} Δ*kar9* cells expressing Ruby-Tub1 and mitoBFP were grown at 24°C or 37°C, as indicated, and visualized by fluorescence microscopy. (A) Representative whole-cell projections of cells with spindles scored as correctly oriented and misoriented are shown. Examples of correctly oriented spindles are from WT cells at 24°C, and examples of misoriented spindles are from *mito*^{ts} and *mito*^{ts} Δ*kar9* at 37°C. (B and C) Quantification of the percentage of cells with misoriented spindles in an otherwise WT (B) or Δ*kar9* background (C) is shown as the mean ± SD. Large buds with

yond Num1 to several proteins that function to establish, maintain, and alter contact between organelles.

Mitochondria-dependent assembly of Num1 is likely driven by multiple, nonmutually exclusive mechanisms. For example, the interaction between Num1 and the MOM may induce conformational changes in Num1 that facilitate Num1–Num1 and Num1–Mdm36 interactions (Lackner et al., 2013). Additionally, Num1's lipid-binding domains may associate with domains on the MOM and plasma membrane that are enriched in the lipid or membrane structure preferred for binding (Yu et al., 2004; Tang et al., 2012; Ping et al., 2016). The preferential binding of Num1 to cardiolipin and $PI_{4,5}P_2$, organelle-specific lipids that play key structural, regulatory, and signaling roles (Strahl and Thorner, 2007; Claypool and Koehler, 2012), may provide a mechanism to integrate Num1 assembly and, thus, its tethering capacity with mitochondrial and cellular functions. Not all circumstances of proximity between mitochondria and the plasma membrane result in the formation of a Num1 cluster, indicating that proximity to the MOM, though necessary, is not sufficient to trigger assembly. Other factors likely contribute to Num1 assembly. One such factor may be the cortical ER, which is present at sites of Num1-mediated mitochondrial tethering (Lackner et al., 2013). In addition, specific features, such as distinct membrane structures, on the mitochondrial surface may be limiting for Num1 assembly (Ping et al., 2016).

Though increasing the avidity of Num1 for its tethering targets is a likely consequence of assembly, Num1 assembly may serve other functions. Num1 is proposed to directly activate dynein by relieving Pac1/LIS1-mediated inhibition (Lammers and Markus, 2015). Thus, increasing the effective concentration of Num1 via cluster formation may enhance dynein activation at sites of anchoring. Whereas nearly all Num1 clusters observed are engaged in mitochondrial tethering (Fig. 1, A and B), only a small subset also functions to anchor dynein (Markus et al., 2009; Markus and Lee, 2011). It is not known whether and how specific Num1 clusters are selected as dynein anchors or whether the process is stochastic. Consistent with a previous study, we observe Num1-mediated dynein anchoring in mother cells as well as daughters (Lee et al., 2003). The function of mother cell–anchored dynein is unclear, and bud-anchored dynein is proposed to be the major contributor to correct spindle orientation (Lee et al., 2003). Consistently, we observe that the bud-specific loss of Num1 clusters results in spindle positioning defects comparable with those observed in the absence of dynein.

Overall, our data demonstrate that the inheritance and positioning of mitochondria influence when and where dynein anchoring can occur, which is critical for dynein's function in mitotic spindle orientation. Therefore, Num1-mediated mitochondria–plasma membrane tethering not only impacts the spatial distribution of mitochondria within cells, but also the position of the spindle, adding a novel function to the growing list of interorganelle contact site functions. Linking both anchoring functions of Num1 to its mitochondria-driven assembly provides a mechanism to spatially and temporally integrate the positioning of two essential organelles. Thus, Num1 assembly serves to regulate a cortical hub that promotes spatial organization within the cell.

Materials and methods

Strains and plasmids

Strains W303 (*ade2–1*; *leu2–3*; *his3–11*, *15*; *trp1–1*; *ura3–1*; *can1–100*) (Naylor et al., 2006), BY4741 (*MATα*; *his3Δ1*; *leu2Δ0*; *ura3Δ0*; *met15Δ0*) (Open Biosystems), W303 *NUM1-yEGFP*::*HIS* and W303 Δ*dyn1*::*HIS* (Lackner et al., 2013), and W303 *NUM1-yEGFP*::*KAN* (Ping et al., 2016) were described previously. BY4741 *mmr1-5*::*HIS3*, Δ*ypt11*::*KAN*, (Chernyakov et al., 2013), and BY4741 *myo2-14*::*HIS* (Santiago-Tirado et al., 2011) were gifts from the A. Bretscher laboratory (Cornell University, Ithaca, NY).

The plasmids pXY142-mitodsRED (mitoRED; Friedman et al., 2011), p412-ADH1 mitoTagBFP (mitoBFP::LEU; Ping et al., 2016), pYX122-mitoGFP::HIS (mitoGFP::HIS) and pYX142-mitoGFP::LEU (mitoGFP::LEU; Westermann and Neupert, 2000), pYES-TagBFP (Murley et al., 2013), pKT127 pFA6-link-yEGFP-KAN and pKT209 pFA6-link-yEGFP-CaURA3 (Sheff and Thorn, 2004), pHyg-AID*-6FLAG (Morawska and Ulrich, 2013), and p416ADH1 (Mumberg et al., 1995) were described previously. pHIS3p:mRuby2-Tub1+3′UTR ::HPH (Ruby-Tub1::HYG) and pHIS3p:mTurquoise2-Tub1+3′UTR ::LEU2 (plasmids 50633 and 50641; Addgene) were gifts from W. Lee (University of Massachusetts, Amherst, MA; Markus et al., 2015). pNHK53 (YIp, ADH1::OsTIR1-9Myc1) (TIR1) was obtained from the National BioResource Project (depositor: M. Kanemaki; Nishimura et al., 2009). pNHK53 was digested with StuI before transformation into yeast. pFA6-link-mKATE-*spHIS5* was a gift from C. Osman and P. Walter (University of California, San Francisco, San Francisco, CA).

p416ADH1 mitoTagBFP (mitoBFP::URA) was constructed by subcloning mitoTagBFP from pYES-TagBFP into p416ADH1 using SpeI and XhoI sites.

pHIS3p:mRuby2-Tub1+3′UTR::LEU (Ruby-Tub1::LEU) was constructed by subcloning HIS3p:mRuby2 from pHIS3p:mRuby2 -Tub1+3′UTR::HPH into pHIS3p:mTurquoise2-Tub1+3′UTR::LEU2 using PacI and BamHI sites. Both Ruby-Tub1::HYG and Ruby-Tub1::LEU were digested with XbaI before transformation into yeast.

The following W303 gene deletion strains were obtained by replacing the complete ORF of the genes with the indicated cassette using PCR-based targeted homologous recombination: Δ*ypt11*::*NATNT2*, Δ*mmr1*::*KANMX6*, Δ*num1*::*KANMX6*, Δ*kar9*::*NATNT2*, Δ*dyn1*::*NAT NT2*, and Δ*mdm36*::*NATNT2* (Longtine et al., 1998; Janke et al., 2004). The functional C-terminally tagged strains *DYN1-mKATE*::*HIS* and *MMR1-AID-FLAG*::*HYG* were constructed by PCR-based targeted homologous recombination using pFA6-link-mKATE-*spHIS5* and pHyg-AID*-6FLAG (Morawska and Ulrich, 2013). Haploid mutant/

spindles >1.25 µm were scored. *n* = 3 independent experiments of >40 spindles for each experiment; p-values for B and C are in comparison with WT cells at the respective temperature; the p-value in parentheses is in comparison with *mito*^{ts} at 37°C. (D–F) WT W303, Δ*dyn1*, Δ*num1*, Δ*mmr1*, Δ*mdm36*, *rho*^{0}, Δ*kar9*, *mito*^{AID}, and *mito*^{AID} Δ*kar9* cells expressing Ruby-Tub1 and mitoGFP were grown in the presence of DMSO or 1 mM auxin, as indicated, and visualized by fluorescence microscopy. Representative whole-cell projections of cells with correctly oriented and misoriented spindles are shown (D) and were quantified (E and F) as described above. Examples of correctly oriented spindles are from *mito*^{AID} and Δ*kar9* cells in the presence of DMSO, and examples of misoriented spindles are from *mito*^{AID} Δ*kar9* cells in the presence of auxin. *n* = 3 independent experiments of >47 spindles for each experiment. (A and D) The cell cortex is outlined with a dashed line. Bars, 2 µm. P-values for E and F are for a comparison with WT cells; the p-value in parentheses is for a comparison with *mito*^{AID} in the presence of auxin; **, P < 0.01; ***, P < 0.001. (G) Quantification of the number of spindles that cross the mother–bud neck over a 10-min time frame in hydroxyurea-arrested WT, Δ*dyn1*, and *mito*^{ts} cells expressing Ruby-Tub1 and mitoGFP grown at 24°C or 37°C, as indicated. *n* ≥ 102 spindles analyzed for each condition.

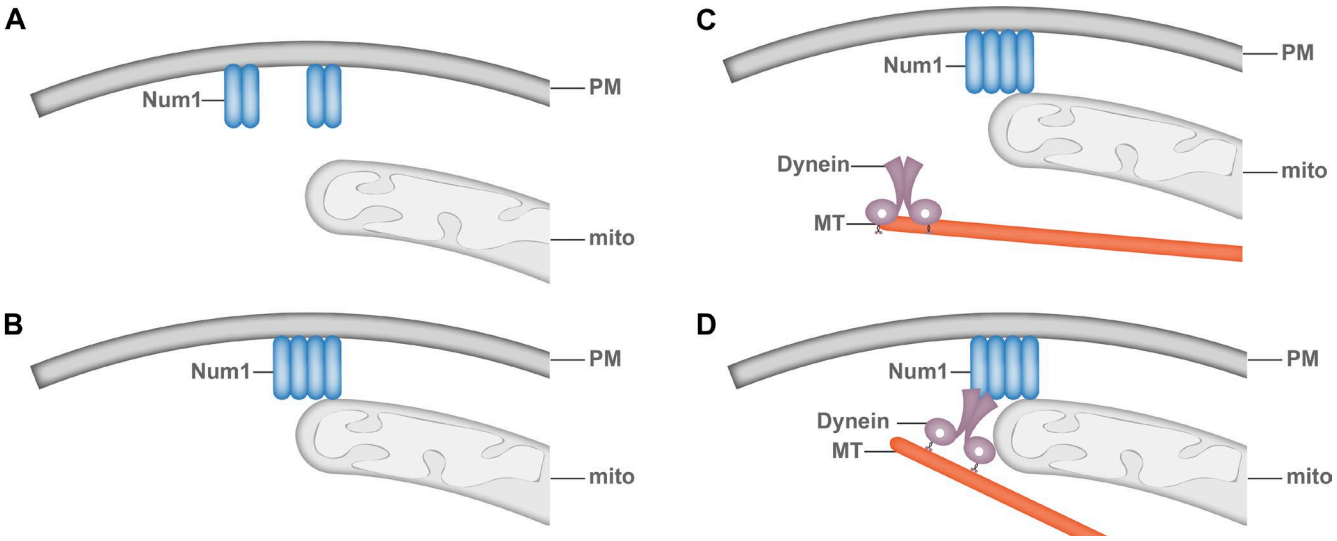

Figure 5. **Model: mitochondria drive the assembly of Num1 clusters, which serve to anchor mitochondria and dynein to the cell cortex.** (A) Num1 dimers associate with the plasma membrane (PM). (B) The assembly of Num1 clusters is triggered by a direct interaction between Num1 and the MOM. Once assembled, Num1 clusters tether mitochondria to the cell cortex. (C) Dynein is trafficked to the cell cortex on microtubules (MTs). (D) Dynein is anchored to the cell cortex by mitochondria-assembled Num1 clusters.

tagged strains were generated by crossing, followed by sporulation and tetrad analysis or by PCR-based targeted homologous recombination. The auxin-inducible mitochondrial inheritance mutant, W303 *MMR1-AID-FLAG* Δ*ypt11 TIR1*, is referred to as *mito*^{AID}. To make the *Num1-yEGFP rho*^{0} mitoRED strain, *Num1-yEGFP* mitoRED cells were grown overnight in synthetic complete (SC) + 2% (wt/vol) dextrose + 25 µg/ml ethidium bromide, diluted, and grown overnight in the same media. Cells were then plated on yeast extract/peptone (YP) + 2% (wt/vol) dextrose (YPD), and loss of mitochondrial DNA was verified by lack of growth on YP + 3% ethanol/3% glycerol plates.

The following BY gene deletion strains were obtained by replacing the complete ORF of the genes with the indicated cassette using PCR-based targeted homologous recombination: Δ*mmr1*::*KANMX6*, Δ*mdm36*::*NATNT2*, Δ*num1*::*NATNT2*, and Δ*kar9*::*NATNT2* (Longtine et al., 1998; Janke et al., 2004). BY Δ*dyn1*::*KANMX6* was obtained from the yeast knockout collection (Open Biosystems). The functional C-terminally tagged *NUM1-yEGFP*::*URA* was constructed by PCR-based targeted homologous recombination using pFA6-link-yEGFP-CaURA3 (Sheff and Thorn, 2004). Haploid mutant/tagged strains were generated by crossing, followed by sporulation and tetrad analysis, or by PCR-based targeted homologous recombination.

Imaging

For Fig. 1, W303 *NUM1-yEGFP* cells harboring mitoRED were grown to midlog phase in SC-LEU + 2% (wt/vol) dextrose media with 2× adenine.

For Fig. 2 and Fig. S1, BY *NUM1-yEGFP*, *mito*^{ts} *NUM1-yEGFP*, and *myo2-14 NUM1-yEGFP* strains harboring mitoRED were grown in SC-LEU + 2% (wt/vol) dextrose media with 2× adenine media at 24°C for 2 h. The permissive temperature cultures were left at 24°C, and the nonpermissive temperature cultures were shifted to 37°C for an additional 4 h of growth.

For Fig. 3 A, W303 *NUM1-yEGFP DYN1-mKATE* cells harboring mitoBFP::URA were grown to midlog phase in SC-URA + 2% (wt/vol) dextrose media with 2× adenine. For Fig. 3 B, W303 *NUM1-yEGFP DYN1-mKATE* cells were grown to midlog phase in SC + 2% (wt/vol) dextrose media with 2× adenine.

For Fig. 4 (A–C), BY WT, Δ*dyn1*, Δ*num1*, Δ*mmr1*, Δ*mdm36*, Δ*kar9*, *mito*^{ts} *NUM1-yEGFP*, and *mito*^{ts} Δ*kar9 NUM1-yEGFP* cells harboring Ruby-Tub1::HYG and mitoBFP::LEU were grown in SC-LEU + 2% (wt/vol) dextrose media with 2× adenine media at 24°C for 2 h. The permissive temperature cultures were left at 24°C, and the nonpermissive temperature cultures were shifted to 37°C for an additional 4 h of growth.

For Fig. 4 (D–F), W303 WT, Δ*dyn1*, Δ*num1*, Δ*mmr1*, Δ*mdm36*, *rho*^{0}, Δ*kar9*, *mito*^{AID}, and *mito*^{AID} Δ*kar9* cells harboring Ruby-Tub1::LEU and mitoGFP::HIS were grown in SC-HIS + 2% (wt/vol) dextrose media with 2× adenine, pH 6.4, media at 30°C for 2 h. DMSO or auxin (α-naphthalene acetic acid; HiMedia), at a final concentration of 1 mM, was added and cells were grown for an additional 3 h at 30°C.

For Fig. 4 G, BY WT, Δ*dyn1*, and *mito*^{ts} cells harboring Ruby-Tub1::HYG and mitoGFP::LEU were diluted from a saturated culture in SC-LEU + 2% (wt/vol) dextrose media with 2× adenine and grown at 24°C for 2 h. Cultures were then grown at 24°C or shifted to 37°C for 2 h. Hydroxyurea was added to a final concentration of 200 mM, and the cells were grown for an additional 2.5 h.

For Fig. S2, W303 *NUM1-yEGFP DYN1-mKATE* cells harboring Ruby-Tub1::LEU were grown to midlog phase in SC + 2% (wt/vol) dextrose media with 2× adenine.

For all imaging, cells were grown as described above at 24°C unless otherwise indicated, concentrated by centrifugation, and mounted on a 4% wt/vol agarose pad. All imaging was performed at 22°C. Because of doubling times of ∼200 min or greater, cell growth was often limited in our imaging conditions. Z series of cells were imaged at a single time point or over time using a spinning disk confocal system (Leica) fit with a spinning disk head (CSU-X1; Yokogawa), a PLAN APO 100× 1.44 NA objective (Leica), and an electron-multiplying charge-coupled device camera (Evolve 512 Delta; Photometrics). A step size of 0.4 µm was used. Image capture was done using Metamorph (Molecular Devices). The images were deconvolved using AutoQuant X3's (Media Cybernetics) iterative, constrained 3D deconvolution method. Fiji (National Institutes of Health) and Photoshop (Adobe) were used to make linear adjustments to brightness and contrast. Deconvolved images are shown. A cluster is defined as an accumulation of Num1 above the background signal that persists for at least three frames of imaging (>1.5 min). The dimmer accumulations of Num1 that do not result in a productive cluster or tether point are dynamic and do not persist over multiple frames. For quantification of tether points, mitochondria had

to remain associated with a Num1 cluster for ≥1.5 min for the cluster to be considered a tether.

For the quantification of spindle orientation, large budded cells with spindles >1.25 µm were analyzed (Moore et al., 2008). Buds were classified as follows: small buds have a bud/mother diameter ratio of <1:3, and large buds have a bud/mother diameter ratio of ≥1:3. To be correctly oriented, the spindle needed to cross the mother–bud neck or be within 45° of a line perpendicular to the neck. Misoriented spindles did not cross the neck and were >45° off of the mother–bud axis. Measurements of bud size, spindle length, and orientation were all done in Fiji. For the spindle oscillation assay, Z stacks were acquired as described above every 30 s for 10 min. Spindles were scored as either crossing the mother–bud neck or not during the course of the 10-min video.

FRAP

Photobleaching was performed on the Leica spinning disk confocal system (described in the previous section) fit with an iLas^2 FRAP module (Roper Scientific). The iLas^2 module is fully integrated into the microscope and driven by Metamorph. A region of interest (ROI) was defined in Metamorph, and the 401-nm laser line was directed to and scanned over the ROI as a diffraction-limited spot using the galvo motors in the iLas^2 module. A Z stack was acquired before bleaching. The bleach sequence lasted 8 ms and was repeated three times. Pre- and postbleach images were captured at 1-s intervals. Because the Num1-yEGFP signal is low, we captured images at 3-min intervals after bleaching to limit photobleaching of the nonbleached regions of the cell. The first Z stack was captured 15 s after photobleaching. Images were deconvolved as described above. All quantification was done in Fiji. 20 × 20–pixel ROIs were drawn for each bleach and control region. A background region was also measured. The mean gray value for each ROI was measured and exported to Excel (Microsoft). The background value was subtracted from each measurement, and all values were normalized to the prebleach value for that experiment (Bolognesi et al., 2016). The normalized values were averaged for all experiments. The mean intensity and SD for each time point were plotted using GraphPad (Prism). For images, Fiji and Photoshop were used to make linear adjustments to brightness and contrast. Deconvolved images are shown.

Western blot

For Fig. S3 A, *mito^{AID}* and *mito^{AID}* Δ*kar9* cells expressing Tir1 and W303 Δ*kar9* cells were grown as described in the Imaging section. Equivalent ODs of cells were taken from all samples before and 3 h after the addition of DMSO or 1 mM auxin. For Fig. S3 D, *mito^{AID} NUM1*-yEGFP cells expressing Tir1 were grown as described in the Imaging section. Equivalent ODs of cells were taken before and 30 min after the addition of DMSO or 1 mM auxin. Whole-cell extracts were prepared using a NaOH lysis and TCA precipitation procedure. Each TCA pellet was resuspended in 50 µl MURB (100 mM MES, pH 7, 1% SDS, and 3 M urea). Whole-cell extracts were analyzed by SDS-PAGE followed by Western analysis using anti-FLAG antibody (Sigma-Aldrich) and anti–glucose-6-phosphate dehydrogenase (G-6-PDH) antibody (Sigma-Aldrich) as the primary antibodies and goat anti–mouse IgG DyLight 680 and goat anti–rabbit IgG DyLight 800 (Thermo Fisher Scientific), respectively, as the secondary antibodies. The immunoreactive bands were detected with the Odyssey Infrared Imaging System (LI-COR Biosciences).

Growth assay

For analysis of growth by serial dilution, cells were grown overnight in YP + 2% (wt/vol) dextrose media, pelleted, and resuspended in water at a concentration of 0.2 OD_{600}/ml, and 10-fold serial dilutions were performed. Cells were spotted onto YPD (Fig. S2) or YPD plus DMSO or 1 mM auxin (Fig. S3) and grown at 30°C.

Online supplemental material

In Fig. S1, *myo2-14*, a temperature-sensitive mitochondrial inheritance mutant, is used to provide additional evidence that Num1 cluster assembly is disrupted in buds that do not inherit mitochondria. Fig. S2 provides evidence that the Dyn1-mKate fusion protein is functional. In Fig. S3, a characterization of the *mito^{AID}* strain is provided.

Acknowledgments

We thank members of the Lackner laboratory, Suzanne Hoppins, Jennifer Brace, and members of the Weiss laboratory for suggestions and critical scientific discussions. We thank Yilan Wang for strain construction. We thank Jessica Hornick and instrumentation support from the Biological Imaging Facility at Northwestern University.

L.M. Kraft is supported by the National Institute of General Medical Sciences training grant T32GM008061. L.L. Lackner is supported by the National Institute of General Medical Sciences grant R01GM120303 and the Robert H. Lurie Comprehensive Cancer Center–Lefkofsky Family Foundation Liz and Eric Lefkofsky Innovation Research Award.

The authors declare no competing financial interests.

Author contributions: L.M. Kraft and L.L. Lackner both contributed to the conception and design of the experiments, the acquisition, analysis, and interpretation of data, and the writing of the manuscript.

Submitted: 3 February 2017
Revised: 1 June 2017
Accepted: 17 July 2017

References

Adames, N.R., and J.A. Cooper. 2000. Microtubule interactions with the cell cortex causing nuclear movements in *Saccharomyces cerevisiae. J. Cell Biol.* 149:863–874. http://dx.doi.org/10.1083/jcb.149.4.863

Altmann, K., M. Frank, D. Neumann, S. Jakobs, and B. Westermann. 2008. The class V myosin motor protein, Myo2, plays a major role in mitochondrial motility in *Saccharomyces cerevisiae. J. Cell Biol.* 181:119–130. http://dx.doi.org/10.1083/jcb.200709099

Boldogh, I.R., S.L. Ramcharan, H.C. Yang, and L.A. Pon. 2004. A type V myosin (Myo2p) and a Rab-like G-protein (Ypt11p) are required for retention of newly inherited mitochondria in yeast cells during cell division. *Mol. Biol. Cell.* 15:3994–4002. http://dx.doi.org/10.1091/mbc.E04-01-0053

Bolognesi, A., A. Sliwa-Gonzalez, R. Prasad, and Y. Barral. 2016. Fluorescence recovery after photo-bleaching (FRAP) and fluorescence loss in photobleaching (FLIP) experiments to study protein dynamics during budding yeast cell division. *Methods Mol. Biol.* 1369:25–44. http://dx.doi.org/10.1007/978-1-4939-3145-3_3

Cerveny, K.L., S.L. Studer, R.E. Jensen, and H. Sesaki. 2007. Yeast mitochondrial division and distribution require the cortical num1 protein. *Dev. Cell.* 12:363–375. http://dx.doi.org/10.1016/j.devcel.2007.01.017

Chao, J.T., A.K. Wong, S. Tavassoli, B.P. Young, A. Chruscicki, N.N. Fang, L.J. Howe, T. Mayor, L.J. Foster, and C.J. Loewen. 2014. Polarization of the endoplasmic reticulum by ER-septin tethering. *Cell.* 158:620–632. http://dx.doi.org/10.1016/j.cell.2014.06.033

Chernyakov, I., F. Santiago-Tirado, and A. Bretscher. 2013. Active segregation of yeast mitochondria by Myo2 is essential and mediated by Mmr1 and Ypt11. *Curr. Biol.* 23:1818–1824. http://dx.doi.org/10.1016/j.cub.2013.07.053

Claypool, S.M., and C.M. Koehler. 2012. The complexity of cardiolipin in health and disease. *Trends Biochem. Sci.* 37:32–41. http://dx.doi.org/10.1016/j.tibs.2011.09.003

Eisenberg-Bord, M., N. Shai, M. Schuldiner, and M. Bohnert. 2016. A tether is a tether is a tether: tethering at membrane contact sites. *Dev. Cell.* 39:395–409. http://dx.doi.org/10.1016/j.devcel.2016.10.022

Eshel, D., L.A. Urrestarazu, S. Vissers, J.C. Jauniaux, J.C. van Vliet-Reedijk, R.J. Planta, and I.R. Gibbons. 1993. Cytoplasmic dynein is required for normal nuclear segregation in yeast. *Proc. Natl. Acad. Sci. USA.* 90:11172–11176. http://dx.doi.org/10.1073/pnas.90.23.11172

Eves, P.T., Y. Jin, M. Brunner, and L.S. Weisman. 2012. Overlap of cargo binding sites on myosin V coordinates the inheritance of diverse cargoes. *J. Cell Biol.* 198:69–85. http://dx.doi.org/10.1083/jcb.201201024

Farkasovsky, M., and H. Küntzel. 1995. Yeast Num1p associates with the mother cell cortex during S/G2 phase and affects microtubular functions. *J. Cell Biol.* 131:1003–1014. http://dx.doi.org/10.1083/jcb.131.4.1003

Farkasovsky, M., and H. Küntzel. 2001. Cortical Num1p interacts with the dynein intermediate chain Pac11p and cytoplasmic microtubules in budding yeast. *J. Cell Biol.* 152:251–262. http://dx.doi.org/10.1083/jcb.152.2.251

Förtsch, J., E. Hummel, M. Krist, and B. Westermann. 2011. The myosin-related motor protein Myo2 is an essential mediator of bud-directed mitochondrial movement in yeast. *J. Cell Biol.* 194:473–488. http://dx.doi.org/10.1083/jcb.201012088

Frederick, R.L., K. Okamoto, and J.M. Shaw. 2008. Multiple pathways influence mitochondrial inheritance in budding yeast. *Genetics.* 178:825–837. http://dx.doi.org/10.1534/genetics.107.083055

Friedman, J.R., L.L. Lackner, M. West, J.R. DiBenedetto, J. Nunnari, and G.K. Voeltz. 2011. ER tubules mark sites of mitochondrial division. *Science.* 334:358–362. http://dx.doi.org/10.1126/science.1207385

Gatta, A.T., and T.P. Levine. 2017. Piecing together the patchwork of contact sites. *Trends Cell Biol.* 27:214–229. http://dx.doi.org/10.1016/j.tcb.2016.08.010

Hammermeister, M., K. Schödel, and B. Westermann. 2010. Mdm36 is a mitochondrial fission-promoting protein in *Saccharomyces cerevisiae*. *Mol. Biol. Cell.* 21:2443–2452. http://dx.doi.org/10.1091/mbc.E10-02-0096

Heil-Chapdelaine, R.A., J.R. Oberle, and J.A. Cooper. 2000. The cortical protein Num1p is essential for dynein-dependent interactions of microtubules with the cortex. *J. Cell Biol.* 151:1337–1344. http://dx.doi.org/10.1083/jcb.151.6.1337

Helle, S.C., G. Kanfer, K. Kolar, A. Lang, A.H. Michel, and B. Kornmann. 2013. Organization and function of membrane contact sites. *Biochim. Biophys. Acta.* 1833:2526–2541. http://dx.doi.org/10.1016/j.bbamcr.2013.01.028

Itoh, T., A. Watabe, A. Toh-E, and Y. Matsui. 2002. Complex formation with Ypt11p, a rab-type small GTPase, is essential to facilitate the function of Myo2p, a class V myosin, in mitochondrial distribution in *Saccharomyces cerevisiae*. *Mol. Cell. Biol.* 22:7744–7757. http://dx.doi.org/10.1128/MCB.22.22.7744-7757.2002

Itoh, T., A. Toh-E, and Y. Matsui. 2004. Mmr1p is a mitochondrial factor for Myo2p-dependent inheritance of mitochondria in the budding yeast. *EMBO J.* 23:2520–2530. http://dx.doi.org/10.1038/sj.emboj.7600271

Janke, C., M.M. Magiera, N. Rathfelder, C. Taxis, S. Reber, H. Maekawa, A. Moreno-Borchart, G. Doenges, E. Schwob, E. Schiebel, and M. Knop. 2004. A versatile toolbox for PCR-based tagging of yeast genes: new fluorescent proteins, more markers and promoter substitution cassettes. *Yeast.* 21:947–962. http://dx.doi.org/10.1002/yea.1142

Klecker, T., D. Scholz, J. Förtsch, and B. Westermann. 2013. The yeast cell cortical protein Num1 integrates mitochondrial dynamics into cellular architecture. *J. Cell Sci.* 126:2924–2930. http://dx.doi.org/10.1242/jcs.126045

Kraft, L.M., and L.L. Lackner. 2017. Mitochondrial anchors: Positioning mitochondria and more. *Biochem. Biophys. Res. Commun.* In press. http://dx.doi.org/10.1016/j.bbrc.2017.06.193

Lackner, L.L., H. Ping, M. Graef, A. Murley, and J. Nunnari. 2013. Endoplasmic reticulum-associated mitochondria-cortex tether functions in the distribution and inheritance of mitochondria. *Proc. Natl. Acad. Sci. USA.* 110:E458–E467. http://dx.doi.org/10.1073/pnas.1215232110

Lammers, L.G., and S.M. Markus. 2015. The dynein cortical anchor Num1 activates dynein motility by relieving Pac1/LIS1-mediated inhibition. *J. Cell Biol.* 211:309–322. http://dx.doi.org/10.1083/jcb.201506119

Lee, W.L., J.R. Oberle, and J.A. Cooper. 2003. The role of the lissencephaly protein Pac1 during nuclear migration in budding yeast. *J. Cell Biol.* 160:355–364. http://dx.doi.org/10.1083/jcb.200209022

Li, Y.Y., E. Yeh, T. Hays, and K. Bloom. 1993. Disruption of mitotic spindle orientation in a yeast dynein mutant. *Proc. Natl. Acad. Sci. USA.* 90:10096–10100. http://dx.doi.org/10.1073/pnas.90.21.10096

Longtine, M.S., A. McKenzie III, D.J. Demarini, N.G. Shah, A. Wach, A. Brachat, P. Philippsen, and J.R. Pringle. 1998. Additional modules for versatile and economical PCR-based gene deletion and modification in *Saccharomyces cerevisiae*. *Yeast.* 14:953–961. http://dx.doi.org/10.1002/(SICI)1097-0061(199807)14:10<953::AID-YEA293>3.0.CO;2-U

Markus, S.M., and W.L. Lee. 2011. Regulated offloading of cytoplasmic dynein from microtubule plus ends to the cortex. *Dev. Cell.* 20:639–651. http://dx.doi.org/10.1016/j.devcel.2011.04.011

Markus, S.M., J.J. Punch, and W.L. Lee. 2009. Motor- and tail-dependent targeting of dynein to microtubule plus ends and the cell cortex. *Curr. Biol.* 19:196–205. http://dx.doi.org/10.1016/j.cub.2008.12.047

Markus, S.M., S. Omer, K. Baranowski, and W.L. Lee. 2015. Improved plasmids for fluorescent protein tagging of microtubules in *Saccharomyces cerevisiae*. *Traffic.* 16:773–786. http://dx.doi.org/10.1111/tra.12276

Miller, R.K., and M.D. Rose. 1998. Kar9p is a novel cortical protein required for cytoplasmic microtubule orientation in yeast. *J. Cell Biol.* 140:377–390. http://dx.doi.org/10.1083/jcb.140.2.377

Moore, J.K., J. Li, and J.A. Cooper. 2008. Dynactin function in mitotic spindle positioning. *Traffic.* 9:510–527. http://dx.doi.org/10.1111/j.1600-0854.2008.00710.x

Moore, J.K., D. Sept, and J.A. Cooper. 2009. Neurodegeneration mutations in dynactin impair dynein-dependent nuclear migration. *Proc. Natl. Acad. Sci. USA.* 106:5147–5152. http://dx.doi.org/10.1073/pnas.0810828106

Morawska, M., and H.D. Ulrich. 2013. An expanded tool kit for the auxin-inducible degron system in budding yeast. *Yeast.* 30:341–351. http://dx.doi.org/10.1002/yea.2967

Mumberg, D., R. Müller, and M. Funk. 1995. Yeast vectors for the controlled expression of heterologous proteins in different genetic backgrounds. *Gene.* 156:119–122. http://dx.doi.org/10.1016/0378-1119(95)00037-7

Murley, A., L.L. Lackner, C. Osman, M. West, G.K. Voeltz, P. Walter, and J. Nunnari. 2013. ER-associated mitochondrial division links the distribution of mitochondria and mitochondrial DNA in yeast. *eLife.* 2:e00422. http://dx.doi.org/10.7554/eLife.00422

Naylor, K., E. Ingerman, V. Okreglak, M. Marino, J.E. Hinshaw, and J. Nunnari. 2006. Mdv1 interacts with assembled dnm1 to promote mitochondrial division. *J. Biol. Chem.* 281:2177–2183. http://dx.doi.org/10.1074/jbc.M507943200

Nishimura, K., T. Fukagawa, H. Takisawa, T. Kakimoto, and M. Kanemaki. 2009. An auxin-based degron system for the rapid depletion of proteins in nonplant cells. *Nat. Methods.* 6:917–922. http://dx.doi.org/10.1038/nmeth.1401

Ping, H.A., L.M. Kraft, W. Chen, A.E. Nilles, and L.L. Lackner. 2016. Num1 anchors mitochondria to the plasma membrane via two domains with different lipid binding specificities. *J. Cell Biol.* 213:513–524. http://dx.doi.org/10.1083/jcb.201511021

Prinz, W.A. 2014. Bridging the gap: membrane contact sites in signaling, metabolism, and organelle dynamics. *J. Cell Biol.* 205:759–769. http://dx.doi.org/10.1083/jcb.201401126

Santiago-Tirado, F.H., A. Legesse-Miller, D. Schott, and A. Bretscher. 2011. PI4P and Rab inputs collaborate in myosin-V-dependent transport of secretory compartments in yeast. *Dev. Cell.* 20:47–59. http://dx.doi.org/10.1016/j.devcel.2010.11.006

Schott, D., J. Ho, D. Pruyne, and A. Bretscher. 1999. The COOH-terminal domain of Myo2p, a yeast myosin V, has a direct role in secretory vesicle targeting. *J. Cell Biol.* 147:791–808. http://dx.doi.org/10.1083/jcb.147.4.791

Sheff, M.A., and K.S. Thorn. 2004. Optimized cassettes for fluorescent protein tagging in *Saccharomyces cerevisiae*. *Yeast.* 21:661–670. http://dx.doi.org/10.1002/yea.1130

Simon, V.R., S.L. Karmon, and L.A. Pon. 1997. Mitochondrial inheritance: cell cycle and actin cable dependence of polarized mitochondrial movements in *Saccharomyces cerevisiae*. *Cell Motil. Cytoskeleton.* 37:199–210. http://dx.doi.org/10.1002/(SICI)1097-0169(1997)37:3<199::AID-CM2>3.0.CO;2-2

Strahl, T., and J. Thorner. 2007. Synthesis and function of membrane phosphoinositides in budding yeast, *Saccharomyces cerevisiae*. *Biochim. Biophys. Acta.* 1771:353–404. http://dx.doi.org/10.1016/j.bbalip.2007.01.015

Tang, X., J.J. Punch, and W.L. Lee. 2009. A CAAX motif can compensate for the PH domain of Num1 for cortical dynein attachment. *Cell Cycle.* 8:3182–3190. http://dx.doi.org/10.4161/cc.8.19.9731

Tang, X., B.S. Germain, and W.L. Lee. 2012. A novel patch assembly domain in Num1 mediates dynein anchoring at the cortex during spindle positioning. *J. Cell Biol.* 196:743–756. http://dx.doi.org/10.1083/jcb.201112017

Westermann, B., and W. Neupert. 2000. Mitochondria-targeted green fluorescent proteins: convenient tools for the study of organelle biogenesis in *Saccharomyces cerevisiae*. *Yeast.* 16:1421–1427. http://dx.doi.org/10.1002/1097-0061(200011)16:15<1421::AID-YEA624>3.0.CO;2-U

Yin, H., D. Pruyne, T.C. Huffaker, and A. Bretscher. 2000. Myosin V orientates the mitotic spindle in yeast. *Nature.* 406:1013–1015. http://dx.doi.org/10.1038/35023024

Yu, J.W., J.M. Mendrola, A. Audhya, S. Singh, D. Keleti, D.B. DeWald, D. Murray, S.D. Emr, and M.A. Lemmon. 2004. Genome-wide analysis of membrane targeting by *S. cerevisiae* pleckstrin homology domains. *Mol. Cell.* 13:677–688. http://dx.doi.org/10.1016/S1097-2765(04)00083-8